

Urban air quality: What is the optimal place to reduce transport emissions?

*Original*

Urban air quality: What is the optimal place to reduce transport emissions? / Li, Tianyang; Fellini, Sofia; van Reeuwijk, Maarten. - In: ATMOSPHERIC ENVIRONMENT. - ISSN 1352-2310. - 292:(2023), p. 119432.  
[10.1016/j.atmosenv.2022.119432]

*Availability:*

This version is available at: 11583/2974159 since: 2022-12-24T11:52:49Z

*Publisher:*

Elsevier

*Published*

DOI:10.1016/j.atmosenv.2022.119432

*Terms of use:*

This article is made available under terms and conditions as specified in the corresponding bibliographic description in the repository

*Publisher copyright*

(Article begins on next page)

# Urban air quality: what is the optimal place to reduce transport emissions?

Tianyang Li<sup>1</sup>, Sofia Fellini<sup>2</sup>, Maarten van Reeuwijk<sup>1,a</sup>

<sup>1</sup> Department of Civil and Environmental Engineering, Imperial College London, SW7 2AZ London

<sup>2</sup> Univ Lyon, INSA Lyon, CNRS, Ecole Centrale de Lyon, Univ Claude Bernard Lyon 1, LMFA,  
UMR5509, 69621, Villeurbanne France.

<sup>a</sup> Email: m.vanreeuwijk@imperial.ac.uk

## Abstract

We develop a linear model based on a complex network approach that predicts the effect of emission changes on air pollution exposure in urban street networks including NO-NO<sub>2</sub>-O<sub>3</sub>-chemistry. The operational air quality model SIRANE is used to create a weighted adjacency matrix  $A$  describing the relation between emissions of a passive scalar inside streets and the resulting concentrations in the street network. A case study in South Kensington (London) is used, and the adjacency matrix  $A_0$  is determined one wind speed and eight different wind directions. The physics of the underlying problem is used to infer  $A$  for different wind speeds. Good agreement between SIRANE predictions and the model is observed for all but the lowest wind speed, despite non-linearities in SIRANE's model formulation. An indicator for exposure in the street is developed, and it is shown that the out-degree of the exposure matrix  $E$  represents the effect of a change in emissions on the exposure reduction in all streets in the network. The approach is then extended to NO-NO<sub>2</sub>-O<sub>3</sub>-chemistry, which introduces a non-linearity. It is shown that a linearised model agrees well with the fully nonlinear SIRANE predictions. The model shows that roads with large height-to-width ratios are the first in which emissions should be reduced in order to maximise exposure reduction.

## 1. Introduction

Almost all the global population (99%) is exposed to pollution levels that exceeds WHO limits, with middle- and low-income countries hit hardest (WHO, 2021). With the progressive shift of people from rural to urban areas, city administrations are urged to develop effective air quality plans to meet air quality standards and protect citizens' health. These plans mainly concern the control of vehicular traffic which is the most important source driving exceedances of air quality standards across city centres (EEA, 2022). For traffic control policies (Lu et al., 2021; Wu et al., 2017) to be effective, it is essential to quantify the contribution of local traffic emissions to the pollution levels of the urban area in order to optimally identify the places to impose restrictions. Methods for quantifying source-receptor relationship are known as source apportionment techniques (Wagstrom et al., 2008; Koo et al., 2009; Clappier et al., 2017) and the most common are based on simulations using air quality models.

Modelling air pollution in urban areas is far from trivial as flow and dispersion dynamics are strongly influenced by the presence of buildings, their geometric properties, and the orientation of the streets. Moreover, polluting emissions and exposure targets (i.e. citizens) are characterized by temporal and spatial patterns that make the analysis more complex. Further modelling issues are encountered when dealing with reactive pollutants. This is the case of nitrogen oxides ( $\text{NO}_2$ ,  $\text{NO}$ ) which are formed in combustion processes (mainly from vehicular traffic) and undergo a series of photochemical reactions with the secondary formation of ozone. Acute exposure to these pollutants causes respiratory diseases and paediatric asthma (Khreis et al., 2017; Anenberg et al., 2022). Since the reaction times of  $\text{NO}_2$ - $\text{NO}$ - $\text{O}_3$  chemistry are comparable to their residence times in the streets (that is governed by turbulent transport) these transformations must be taken into account to predict air pollution at the district and street scales (Derwent & Middleton, 1996; Mchugh et al., 1997; Soulhac et al., 2011) and its impact on citizen's health.

Computational fluid dynamic (CFD) simulations can be effectively used to model flow, dispersion, and chemical reactions (Baker et al., 2004; Bright et al., 2013; Grylls et al., 2019; Zhang et al., 2020) in complex geometries. However, they are computationally expensive and require a large amount of detailed input data. The adoption of simplified modelling techniques is the most efficient option when dealing with urban areas consisting of hundreds of streets and when the goal is to explore multiple emission and exposure scenarios.

To this aim, street network models have been developed in the last decades (Berkowicz, 2000; Kim et al., 2018; McHugh et al., 1997; Soulhac et al., 2011). These are operational tools for air quality modelling based on the description of the urban fabric as a network of streets of homogeneous pollutant concentration. Each street is characterized by a polluting source and by the average geometric properties of the buildings. In this way, the complex urban pattern of buildings is represented by a simplified and regular domain of links (the streets) and nodes (street intersections). The wind flow and the turbulence in streets and street intersections are modelled by parametric relations on the network, while the concentration in the streets is estimated by a mass flow balance. Street network models have proven to be efficient for rapid prediction of air quality over large urban domains (Kakosimos et al., 2010; Soulhac et al., 2011).

Fellini et al., 2019 developed a propagation model on networks to simulate pollutant dispersion from a point source using the same geometrical description as street network models. They used tools and metrics from complex network theory (Fellini et al., 2020, 2021) to unveil the physical mechanisms that drive dispersion processes and to detect vulnerable locations where a toxic gaseous release can

cause the greatest impact. In this paper, a similar methodology is used to predict the optimal location to reduce traffic emissions.

The theory of complex networks aims to describe a system as a network of interactions between its elements. These elements are represented by nodes, interconnected by links whenever a relationship is observed between the corresponding elements. The resulting network can then be described by means of multiple metrics or used as a basis for modelling. This theory has been successfully adopted in the field of urban science to investigate the topological properties of cities but also mobility patterns of citizens and socio-economic dynamics (Batty, 2013; Barthélemy, 2016). Recently, the complex network approach has proved useful in the study of geophysical flows, for example to analyse the motion of particles in turbulent flows (Iacobello et al., 2019; Ser-Giacomi et al., 2019).

Given the complexity of transport and transformation processes of pollutants in the urban atmosphere and the multiplicity of meteorological, emission and exposure scenarios, we propose in this work a network approach to model the relation between pollutant emissions and their impact on citizens and to perform source apportionment analyses. The aim is to answer the question: if a borough would like to reduce emissions in a neighborhood by a certain percentage, on which streets should action be taken in order to maximise the reduction in citizen's exposure? It will be demonstrated that due to the representation of emissions, air quality and exposure in the form of a complex network, multiple emissions and exposure scenarios can be easily simulated and the fundamental elements of the phenomenon are clearly identified.

The work is organized as follows: in section 2 the construction of the network is outlined together with the fundamental concepts of the model. Section 3 presents the case study to which the methodology is applied. Section 4 shows the potential of the model when dealing with a passive pollutant. In section 5, the method is extended to study exposure to reactive pollutants. Finally, in section 6, the conclusions and perspectives of the work are presented.

## 2. Methodology

### 2.1 Complex network representation

A weighted and directed network (Boccaletti et al., 2006) is adopted to model the correlation between pollutant emissions and concentration in the streets. In classical street network models, the network mimics the geometry of the urban fabric, with streets represented as links connecting two nodes that correspond to street intersections (Figure 1.a). Conversely, nodes represent here the streets while the directed links are the emission-impact relation between streets. Therefore, distant streets can also be connected (Figure 1.c) differently from the physical network of streets that is limited by the urban shape. The structure of the network is mathematically described by the adjacency matrix whose elements have a value equal to 1 or 0 depending on whether the pairs of nodes are connected or not in the graph. In addition to this information, the weight matrix  $A$  expresses for each non-zero value the weight (i.e. the importance) associated with the connection (Figure 1.d). The link weights therefore contain all the information relating to the transport of pollutants from one street to another.

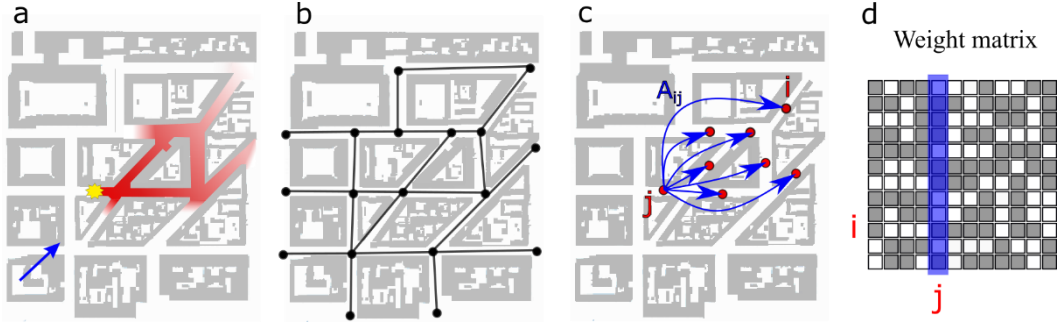


Figure 1: Schematic representation of pollutant dispersion in a dense city (a), the classical street-network domain (b), the emission-concentration network considered in this work (c) and the corresponding weight matrix (d). The non-zero elements in the blue column collect the concentration values in the contaminated streets from node  $j$ .

The main assumption underlying this work is that to first order, the transport within and between the streets can be represented as:

$$\mathbf{C} = \mathbf{A}\mathbf{Q} \quad (1)$$

where  $\mathbf{Q}$  and  $\mathbf{C}$  are the emission and concentration in each street respectively, and  $A_{ij}$  is an entry of the weight matrix that represents how emissions in street  $j$  result in concentrations in street  $i$ . Denoting the number of streets by  $N$ ,  $\mathbf{A}$  is of size  $N \times N$ . Eq. (1) assumes that there is a linear relation between emissions and concentration, which is a hypothesis that will be tested later in the paper. Chemistry will create a nonlinear relation between  $\mathbf{Q}$  and  $\mathbf{C}$ . This issue will be dealt with in Section 5. We note that Eq. (1) is equivalent to a source apportionment method as each row of  $\mathbf{A}$  represents the linear weights of the sources contributing to the concentration in a street of the network.

## 2.2 Construction of the weight matrix $\mathbf{A}$

The weight matrix  $\mathbf{A}$  in Eq. (1) is constructed using the model SIRANE. SIRANE is an operational street network model for urban dispersion that has been adopted in several European cities and has been validated against both wind tunnel experiments and field campaigns (Carpentieri et al., 2012; Soulhac et al., 2003, 2012, 2017). The model is based on a simplified description of the urban geometry and adopts parametric relations to simulate the transport mechanisms of pollutants within the urban canopy. The streets of a city district are modelled as a network of boxes within which the pollutant is assumed to be uniformly mixed. The model simulates three main transport mechanisms: advection along the street axis ( $Q_{adv}$ ), turbulent vertical exchange at the interface between the street and the overlying atmosphere ( $Q_{H,turb}$ ), and exchange at street intersections ( $Q_I$ ). The main physico-chemical processes are also modelled. These are the null-cycle chemistry and wet ( $Q_{wash}$ ) and dry deposition ( $Q_{part}$ ). The mass balance over each street volume for a passive scalar can be written as:

$$Q + Q_I = Q_{H,turb} + Q_{adv} + Q_{part} + Q_{wash}. \quad (2)$$

Above roofs, a Gaussian plume model is used. The interaction between the dispersion above roof and inside the street is mainly taken into account in the term  $Q_{H,turb}$ . SIRANE requires as input data the urban geometry, the meteorological conditions of the site, the background concentration of pollutants and the emissions within the streets. A meteorological pre-processor utilises parametrisations to simulate the boundary layer above roofs from the assigned conditions (Soulhac et al., 2011).

To construct the weight matrix  $\mathbf{A}$ , we perform simulations with SIRANE on the urban district that will be presented in Section 3. We assume that the background concentration is zero and that the only polluting source in the streets is the release of a gas behaving like a passive scalar. This is achieved using an ozone ( $O_3$ ) emission in SIRANE, which, without the presence of any  $NO$  and  $NO_2$ , is an inert

tracer in the model. We perform the simulations at a single wind speed  $U$  and one wind direction  $\phi$  at a time. Under these assumptions, the  $j$ -th column of the weight matrix (Figure 1.c-d) is filled by simulating a unit ozone emission in the  $j$ -th street of the network. The resulting concentration values in street network provides column  $j$  of matrix  $A$ . By repeating this operation for all the streets of the network,  $A$  is obtained. This procedure is then repeated for 8 wind directions, and  $A$  therefore depends on the intensity and direction of the wind above roofs, i.e.  $A = A(U, \phi)$ . In practice,  $A$  is determined for one wind speed only, which we will refer to as the reference velocity  $U_0$  and associated weight matrix  $A_0$ . The physics of the problem can be used to infer  $A$  at other wind speeds (see section 4.2).

### 2.3 Exposure

To find the best place to reduce emissions in the urban district, a metric is required that quantifies the exposure of citizens. Personal exposure depends sensitively on the type of pollutant, inhalation rate and duration of the exposure. Here, we adopt a simple measure for the exposure in a street  $e_i$  [g/hr] as:

$$e_i = p_i C_i q, \quad (3)$$

where  $p_i$  is the number of people living in street  $i$  (note that summation over repeated indices is not implied here) and  $q$  is the inhalation rate of a person, which is taken to be 0.571 m<sup>3</sup>/hr (Epa & Factors Program, 2011). In matrix notation, this can be written as

$$\mathbf{e} = \mathbf{q} \mathbf{p} \circ \mathbf{C} = \mathbf{q} \mathbf{p} \circ \mathbf{A} \mathbf{Q} = \mathbf{E} \mathbf{Q}, \quad (4)$$

where  $\circ$  is the Hadamard product and  $E_{ij} = q p_i A_{ij}$  is the exposure matrix. In this work, we will assume that the number of people  $p_i$  is constant as a function of time, but note that it is straightforward to consider different, more complex, scenarios (different days of the week, different hours) by changing the  $\mathbf{p}$  vector only.

### 2.4 Street population estimation

To estimate the number of citizens in each street ( $p_i$ ), we assume that the street is flanked by two buildings of constant width  $w$ , of length equal to the length of the street ( $L_i$ ), and of height equal to the average depth of the street canyon  $H_i$  (panel c in Figure 2). We then assume a constant storey height  $H_F$  to assess the number of floors. The total living space for a street is thus given by:

$$S_i = 2 \frac{H_i L_i w}{H_F}. \quad (5)$$

The corresponding resident population ( $p_i$ ) can be calculated as the ratio between the living space and the average area per capita  $S_p$ , i.e. the average living space for a resident. This latter can be evaluated for a specific district as the ratio of the total living area given by the buildings in the district  $\sum_j 2 H_j L_j w / H_F$  and the number of citizens  $n_{TOT}$  living in the district. Assuming a constant width for the buildings, we obtain the following expression for the number of people in street  $i$ :

$$p_i = 2 \frac{H_i L_i w}{H_F} \frac{n_{TOT}}{2 w \sum_j H_j L_j / H_F} = \frac{H_i L_i}{\sum_j H_j L_j} n_{TOT}. \quad (6)$$

## 3. South Kensington case study

The case study (latitude 51.4998, longitude -0.1748) is located in South Kensington, a district west of central London, UK (Figure 2). The study area spans 672x1344 m<sup>2</sup> between Hyde Park and South

Kensington station and is characterized by high population, developed transport and dense buildings. The high variety of morphological features (e.g., length of the streets, height of the buildings) and the different population density of the building blocks make this area suitable for investigating which places are most sensitive to the reduction of polluting emissions.

The representation of the urban district in SIRANE is detailed in Grylls et al., 2019. The street network is composed of 46 streets that are represented as straight links with starting and ending points located at the centre of the connecting intersections. Consistent with the description of the street as a box (see Section 2.2), each street has average geometric properties associated with it. The height ( $H$ ) is given by the average height of the side buildings, while the street width ( $W$ ) is the average distance between the lateral buildings (see Figure 2). Street length ( $L$ ) is simply the distance between the two street intersections.

The geometrical properties of the street canyons are used to estimate the resident population according to Eq. (6). The total number of citizens  $n_{TOT}$  is estimated as the product of the district area and the average population density ( $12876 \text{ } peo/km^2$ ) of the reference region (Kensington and Chelsea) derived from Park (2020).

To construct the matrix  $A$  for the study area, the simulations with SIRANE are performed with typical meteorological conditions: a temperate night ( $T = 4 \text{ } ^\circ\text{C}$ ) in neutral stability conditions with cloud cover (5 Oktas) and no precipitation. The night condition is adopted to simulate the dispersion of ozone as a passive scalar (see Section 2.2). Starting from these assigned conditions, SIRANE uses parametrizations to estimate the characteristic properties of the boundary layer as well as the reaction rates for reactive pollutants (see Section 5).

Vehicular emissions in the streets are estimated through the coupling of a VISSIM traffic microsimulation (Bloomberg & Dale, 2000) and the emission model developed by Int Panis et al. (2006). The resulting second-by-second  $\text{NO}_x$  emissions are time averaged over 1 hour and spatially averaged over the street boxes. Details are provided in Grylls et al. (2019).

For the passive scalar analysis, the background concentration was taken equal to zero (see also Section 2.1). For the reactive scalar analysis, realistic background concentrations were used. These were obtained as the average value in the 2021 for the reference region (Kensington and Chelsea):  $\text{NO}_2 = 34.26 \text{ } \mu\text{g}/\text{m}^3$ ,  $\text{NO} = 17.09 \text{ } \mu\text{g}/\text{m}^3$  (UK Ambient Air Quality Interactive Map),  $\text{O}_3 = 27.31 \text{ } \mu\text{g}/\text{m}^3$  (Greater London Authority). It is worth noting that the ozone estimate is an eight-hour average. To simulate photochemical reactions, a sunny day ( $T=14 \text{ } ^\circ\text{C}$ ) at noon was considered in this case.



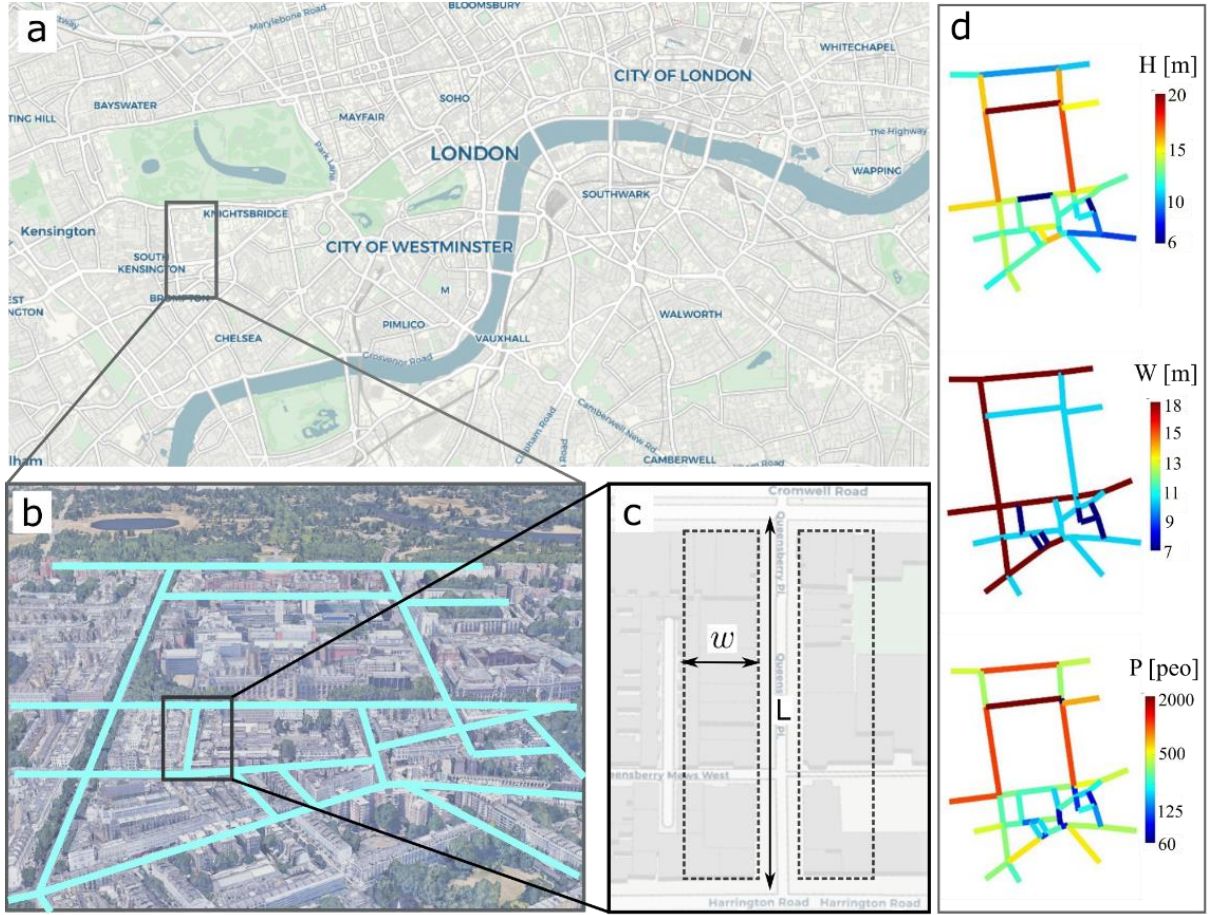


Figure 2: a) Location of South Kensington district in Central London. b) The study area and its street network. c) Schematization of lateral buildings for the estimation of the population. d) Depth ( $H$ ) and width ( $W_s$ ) of the street canyons and estimated population in the streets ( $P$ ).

## 4. Passive scalar transport

### 4.1 Concentration reconstruction

Following the method explained in Section 2.2, we construct the weight matrix  $A$  for the South Kensington district for eight different wind directions, assuming a constant wind speed  $U_0=5$  m/s. In order to verify whether the resulting matrix is correct, we then perform a simulation in SIRANE with random emissions in multiple streets simultaneously (i.e. a random  $Q$  vector) and we compare the results with the concentration in the streets estimated using the linear model presented in Eq. (1). This comparative test is repeated 20 times and the results are reported in Figure 3(a), where each point represents the concentration in a single street for a specific wind direction and for an initial random distribution of emissions. The results show an excellent match between the two models and suggest that the linear assumption holds in the case of passive pollutants emitted in a rainless day (i.e. neglecting chemical reactions and dry and wet deposition) and with negligible re-entrainment of pollutants dispersed above roof levels. In fact, in this case the balance in Eq. (2) can be rewritten as:

$$Q + Q_I = Q_{H,turb} + Q_{adv} \rightarrow Q + U_S W H C_{up} = u_d W L C + U_S W H C, \quad (7)$$

where  $U_S$  and  $u_d$  are the advective velocity along the street canyon and the rate of vertical turbulent transfer at roof level,  $C$  and  $C_{up}$  are the average concentration in the street and in the airflow entering the street from the upwind intersection. The latter is in turn given by a linear superposition of the



emissions in the upwind streets. These considerations evidence that the balance in Eq. (7) can be formulated as Eq. (1) and validate the very good correlation in Figure 3(a).

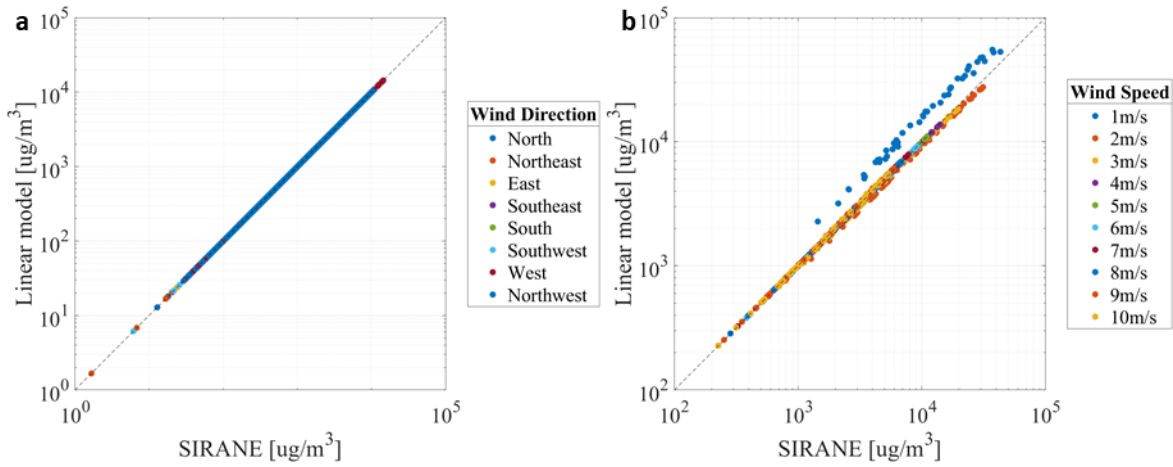


Figure 3: a) Concentration in the streets predicted by SIRANE and by the linear model proposed in Eq. (1) for different wind direction and a constant wind intensity (5 m/s). b) Accuracy as a function of wind speed.

#### 4.2 Wind speed correction

As highlighted by Eq. (7), the wind intensity affects the pollutant balance in the street by means of the two characteristic velocities  $U_s$  and  $u_d$ . Both these velocities can be parameterized as linear functions of the friction velocity ( $u_*$ ) of the overlying boundary layer (Salizzoni et al., 2009 and Soulhac et al., 2010). Furthermore, assuming that the weather conditions are constant over the area of interest, the ratio between  $u_*$  and the free stream velocity ( $U$ ) of the boundary layer is constant. These considerations suggest that matrix  $A$  in Eq. (1) is inversely proportional to the wind intensity  $U$ . Therefore, we can generalise the weight matrix  $A$  for a general wind speed as:

$$A(U, \phi) = \frac{U_0}{U} A_0(U_0, \phi) \quad (8)$$

where  $U_0$  is the reference velocity (5 m/s in this study) and  $A_0$  is the corresponding weight matrix. This scaling is adopted to simulate scenarios with ten different wind intensities, by using Eqs. (1) and (8). As for the reference case, random emissions  $Q$  are prescribed in the streets. The concentration predictions of Eq. (8) are compared in Figure 3(b) with the outcomes of the simulations performed with SIRANE. For each wind intensity, we take the average over the eight wind directions ( $\phi$ ). At low wind speed, the dispersion of pollutants above roof level has a significant impact. For very low wind speeds, the pollution transport above the streets via plumes become important which do not scale as Eq. (8); this leads to inaccuracies in the proposed approximation.

#### 4.3 Diagonal dominance of $A$

In this section we explore the diagonal dominance of matrix  $A$ , which is satisfied when  $|A_{ii}| / \sum_{j \neq i} |A_{ij}| > 1$ , i.e. the matrix is diagonally dominant when, for each row, the magnitude of the diagonal element in a row is larger than or equal to the sum of the magnitudes of all the other entries in that row. If  $A$  is found to be diagonally dominant, the concentration in the streets is mainly affected by local emissions. It should be noted that  $|A_{ii}| / \sum_{j \neq i} |A_{ij}|$  tends to infinity as the matrix becomes diagonal. Therefore, to obtain a useful measure for the matrix as a whole, the harmonic mean of  $|A_{ii}| / \sum_{j \neq i} |A_{ij}|$  for all the rows is taken:

$$D = \left( \frac{1}{N} \sum_i \frac{\sum_{j \neq i} |A_{ij}|}{|A_{ii}|} \right)^{-1}. \quad (9)$$

If  $D > 1$  then the matrix is diagonally dominant on average. The harmonic mean weighs the smallest row values highest and will thus be a conservative estimate. By calculating  $D$  for all eight wind directions, we find that  $133 < D < 193$ , and thus conclude that self-interactions are expected to be very strong. Substitution of Eq. (8) shows that  $D$  is independent of wind velocity (provided the wind speed is not too small).

#### 4.4 Reducing network complexity

The network contains a large number of links due to the transport of pollutants out of street canyons via the atmosphere and into street canyons downwind. The pollutant plume dilutes rapidly with downstream distance, resulting in a large number of very weak links. These can be removed without a noticeable impact on the concentration predictions. As demonstrated in the previous section, the matrix  $A$  is diagonally dominant, and we can use the mean of the diagonal entries to quantify the dominant interactions. We select a geometric mean  $(\prod_1^N A_{ii})^{\frac{1}{N}}$  to avoid one street dominating the mean as the diagonal entries can vary greatly in magnitude depending on the street properties. Introducing a threshold value  $\alpha$ , the modified weight matrix  $\tilde{A}_{ij}$  is determined as:

$$\tilde{A}_{ij} = \begin{cases} A_{ij}, & \text{if } A_{ij} > \alpha \left( \prod_1^N A_{ii} \right)^{\frac{1}{N}} \\ 0, & \text{otherwise} \end{cases} \quad (10)$$

Figure 4 (blue curve) shows the trend in the number of links of matrix  $\tilde{A}_{ij}$  as a function of  $\alpha$ : using a threshold value  $\alpha = 0.01$  decreases the number of links by a factor 3.28. To quantify the error made due to link removal, we consider the relative error in the predicted concentration:

$$\epsilon = \frac{\|c - \tilde{c}\|_2}{\|c\|_2} = \frac{\|(A - \tilde{A})Q\|_2}{\|AQ\|_2} \approx \frac{\|A - \tilde{A}\|_2}{\|A\|_2}$$

where  $\|\cdot\|_2$  is the  $L_2$ -norm, and the last step involves a change from a vector norm to a matrix norm. The red curve in Figure 4 evidence that the relative error  $\epsilon$  is about 0.01 at  $\alpha = 0.01$ , and 0.05 at  $\alpha = 0.1$ . This demonstrates that the number of links can be reduced severely without significantly altering the properties of  $A$ . For large networks, using a small threshold value  $\alpha$  will imply substantial savings in memory and an increase in computational performance. However, since the network considered here is small, we will not make use of the simplification.

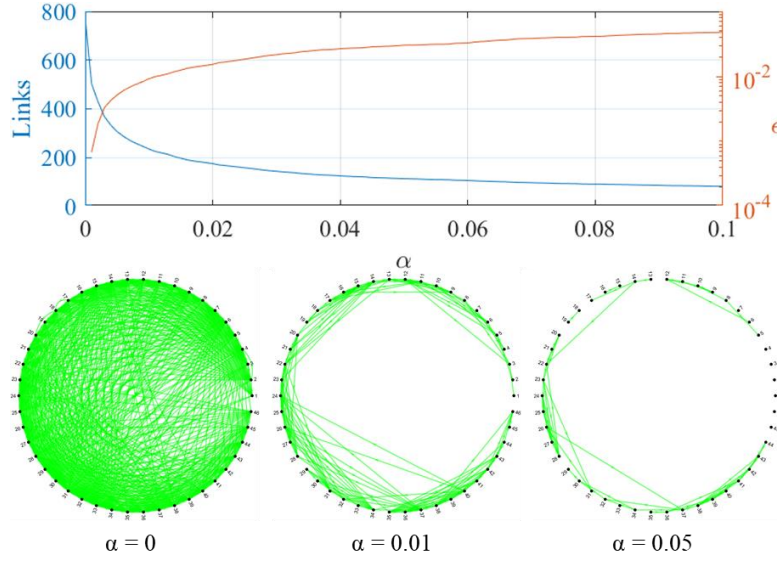


Figure 4: Number of links and error ( $\epsilon$ ) due to link removal for networks with different exclusive threshold  $\alpha$ .

#### 4.5 Where to reduce emissions?

The scenario considered here is that a borough decides to reduce its total emissions by a certain amount and would like to know in which street this should be done in order to have the largest health benefits for its citizens. To answer this question, it is necessary to quantify the contribution of the emission in each street to the air pollution in the urban area. The process of evaluating the effect of a single source on the total concentrations is called source apportionment.

Following the source apportionment strategy, and in particular the tagged species approach (Wang et al., 2009; Grewe et al., 2010), we perturb the emission-exposure model introduced in Section 2 to analyse the exposure variation due to a change in the pollutant emissions as:

$$\delta e = E \delta Q. \quad (11)$$

The desired emission change is assumed to be  $\delta Q = b \bar{Q}$  where  $\bar{Q} = \frac{1}{N} \sum_i Q_i$  is the average emission rate per street and  $b$  is a parameter, which is taken to be 0.10 here. We are looking for the street  $j$  whose emission reduction  $-\delta Q$  maximizes the sum of the exposure change in all the streets. The total exposure reduction  $R_j$  due to an emission reduction  $\delta Q_j = -\delta Q$  in street  $j$  can be expressed by:

$$R_j = -\sum_i \delta e_i = -\sum_k \delta Q_k \sum_i E_{ik} = \delta Q \sum_i E_{ij} \quad (12)$$

where the last step uses that  $\delta Q$  is different from 0 only in street  $j$ . Note that  $\sum_i E_{ij}$  is the outdegree of node  $j$  ( $d_j^+$ ) (Newman, 2010). So, the optimal place to reduce emissions corresponds to the node with the highest outdegree in the defined weighted network.

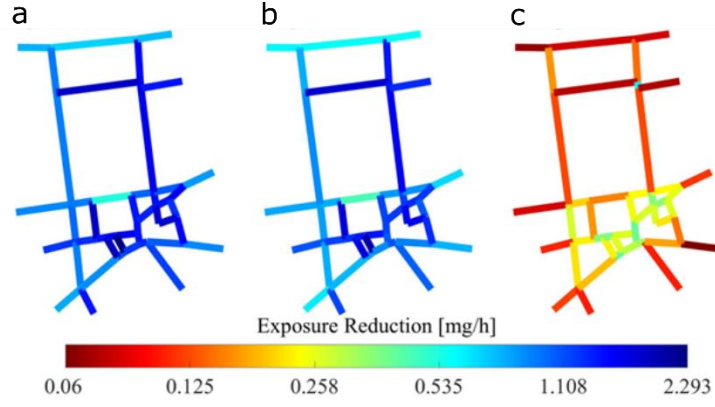


Figure 5: Exposure reduction achieved by decreasing the emission in the street by a constant quantity  $\delta Q$ . Panels a and b show the maximum and average values for the different wind directions. Panel c shows the average computed by neglecting self-interactions.

The exposure reduction ( $\mathbf{R}$ ) is shown in Figure 5. In the analysis, we consider a single wind intensity  $U_0 = 5$  m/s since we are interested in the variability of  $\mathbf{R}$  among the streets and not in its absolute value. In this sense, the results shown in Figure 5 are also valid for the other wind intensities, in accordance with the linear relation in Eq. (8). Panels a and b show the maximum and average  $\mathbf{R}$  for the different wind direction scenarios. The similarity between the two figures suggests that the results depend only weakly on the wind direction. This is likely because the main exposure reduction occurs in the same street where the emission is limited since matrix  $A$  (and thus  $E$ ) is strongly diagonally dominant, as was shown in Section 4.3. To clarify this point, we report in panel c the results obtained by neglecting self-interactions in matrix  $E$ , i.e. for each street we compute the exposure reduction that is achieved in the whole network except in the street where the emission is reduced. The value of  $\mathbf{R}$  is considerably lower in this case, confirming the importance of self-interactions.

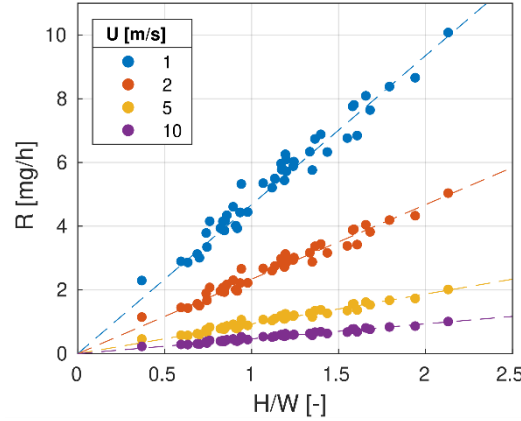
The variability in the exposure reduction among the streets can be related to the geometry of the street canyons and their connectivity. When only self-interactions are considered (panel a and b), Eq. (12) can be evaluated exactly:

$$R_i = \delta Q E_{ii} = \delta Q q p_i \frac{U_0}{U} A_{0,ii} = \frac{U_0}{U} \frac{\delta Q q p_i}{u_{d0} W_i L_i} = \frac{U_0}{U} \frac{\delta Q q n_{TOT}}{u_{d0} \sum_j H_j L_j} \frac{H_i}{W_i}. \quad (13)$$

The exposure reduction will be higher the higher the  $E_{ii}$  entry. This increases with the resident population in the street ( $p_i$ ) and with the entry  $A_{ii}$  which provides the increase in pollutant concentration per unit emission. According to Eq. (6),  $p_i$  is a linear function of the length of the street and the height of the buildings. Following the model reported in Eq. (7) and considering that there is no pollutant exchange at street intersections, we find that  $A_{ii}$  (here reported for a general wind intensity, i.e.  $A = A_0 U_0 / U$ ) decreases with  $W$  and  $L$ . Consequently, as demonstrated in Eq. (13), the exposure reduction is expected to scale with the street aspect ratio  $H/W$ , while the contribution of the street length should be negligible. This is confirmed by Figure 6, which shows a linear trend of the exposure reduction with the canyon aspect ratio for the different scenarios of wind intensity ( $U$ ). The dashed lines correspond to the prediction in Eq. (13). Panels a and b of Figure 5 evidence that  $R_j$  is not dependent on the street length.

When self-interactions are neglected (panel c), the exposure reduction in Eq. (12) is high when  $E_{ij}$  is different from zero for many  $j$ , i.e., when the interconnectivity of the network is high. For this reason, the largest exposure reductions in panel c are obtained on the well interconnected streets of the network.

333



334

335 *Figure 6: Exposure reduction (average over the wind directions) as a function of the aspect ratio (H/W) of the streets.*  
 336 *Dashed lines correspond to the prediction in Eq. (13),*

337

### 338 5. Extension to photochemical smog

339 The formalism will now be extended to include chemically reacting species, namely the NO – NO<sub>2</sub> –  
 340 O<sub>3</sub> cycle associated with photochemical smog (Oke et al., 2017). We follow SIRANE by assuming that  
 341 the characteristic time scales of the chemical reactions are small compared to the residence time of  
 342 pollutants within the streets. Under this assumption, a two-step method can be used to model the  
 343 fate of the chemical species. First, we consider that ozone, nitric oxide and nitrogen dioxide are  
 344 transported passively across the street network. After reaching the designated street, we assume that  
 345 the species are in a photochemical steady state inside the canyon, and we apply chemical reactions to  
 346 obtain the final concentration.

347 Adopting the network approach, the first step is the passive redistribution of chemical species, given  
 348 by

$$\tilde{c}_{NO_2} = Aq_{NO_2}, \quad \tilde{c}_{NO} = Aq_{NO}, \quad \tilde{c}_{O_3} = Aq_{O_3}. \quad (14)$$

349

350 Written in a single matrix multiplication, this becomes

$$\begin{bmatrix} \tilde{c}_{NO_2} \\ \tilde{c}_{NO} \\ \tilde{c}_{O_3} \end{bmatrix} = \begin{pmatrix} A & 0 & 0 \\ 0 & A & 0 \\ 0 & 0 & A \end{pmatrix} \begin{bmatrix} q_{NO_2} \\ q_{NO} \\ q_{O_3} \end{bmatrix}, \quad \text{or simply } \tilde{\mathbf{c}} = B\mathbf{q}. \quad (15)$$

351 The second step is to apply the chemistry which can be represented by

$$\mathbf{c} = \mathbf{f}(\tilde{\mathbf{c}}), \quad (16)$$

352 where  $\mathbf{f}$  is a nonlinear function that maps  $\tilde{\mathbf{c}}$  to  $\mathbf{c}$  in each street. The null-cycle chemistry (Oke et al.,  
 353 2017) together with the conservation of  $N$  and  $O$  species in a single street results in the following  
 354 equilibrium concentrations:

$$[O_3] = \frac{-(k_3(c_N - c_O) + k_1) + \sqrt{\Delta}}{2k_3},$$

$$\begin{aligned} [\text{NO}_2] &= c_O - [\text{O}_3], \\ [\text{NO}] &= c_N - [\text{NO}_2] = c_N - c_O + [\text{O}_3], \end{aligned} \quad (17)$$

where

$$\begin{aligned} c_N &= [\widetilde{\text{NO}}] + [\widetilde{\text{NO}}_2] + [\text{NO}]_b + [\text{NO}_2]_b, \\ c_O &= [\widetilde{\text{NO}}_2] + [\widetilde{\text{O}}_3] + [\text{NO}_2]_b + [\text{O}_3]_b, \\ \Delta &= (k_3(c_N - c_O) + k_1)^2 + 4k_1k_3c_O. \end{aligned} \quad (18)$$

Here, the brackets denote molar concentrations, that are linked to the mass concentrations as  $\tilde{X} = M_X[X]$ , where  $M_X$  is the molar mass (g/mol) of species  $X$ .  $k_1$  is the rate (expressed in  $\text{m}^3\text{mol}^{-1}\text{s}^{-1}$ ) of  $\text{NO}_2$  regeneration from  $\text{NO}$  and  $\text{O}_3$  reaction, and  $k_3$  is the photolysis rate of  $\text{NO}_2$  (expressed in  $\text{s}^{-1}$ ). Denoting  $\tilde{\mathbf{c}} = [\widetilde{\text{NO}}, \widetilde{\text{NO}}_2, \widetilde{\text{O}}_3]^T$  and  $\mathbf{c} = [\text{NO}, \text{NO}_2, \text{O}_3]^T$  as the mass concentration vectors in a single street before and after the chemical reaction, respectively, the relation between the two can be expressed as

$$\mathbf{c} = \mathbf{f}_s(\tilde{\mathbf{c}}) = \mathbf{f}_s(\widetilde{\text{NO}}, \widetilde{\text{NO}}_2, \widetilde{\text{O}}_3), \quad (19)$$

where

where  $\mathbf{f}_s$  represents  $\mathbf{f}$  for a single street. There are a few specifics of air quality simulations that simplify the calculation of the term  $\mathbf{f}_s$ . First, ozone is a secondary pollutant, which implies that it is formed from reactions with primary pollutants and thus  $\mathbf{Q}_{\text{O}_3} = \mathbf{0}$ , which in turn implies that  $\widetilde{\text{O}}_3 = 0$  (see Eq. (14)). Second, the emissions of  $\text{NO}$  and  $\text{NO}_2$  are typically prescribed in terms of an emission ratio  $a = Q_{\text{NO}_2}/Q_{\text{NO}_x}$  where  $a$  is a constant and  $Q_{\text{NO}_x}$  is reported on a  $\text{NO}_2$  basis (i.e. it is assumed that all  $\text{NO}$  is converted to  $\text{NO}_2$ ). This means that

$$\mathbf{Q}_{\text{NO}} = (1 - a) \frac{M_{\text{NO}}}{M_{\text{NO}_2}} \mathbf{Q}_{\text{NO}_x}, \quad \mathbf{Q}_{\text{NO}_2} = a \mathbf{Q}_{\text{NO}_x}, \quad (20)$$

and,

because of the linearity of  $A$ , that  $\widetilde{\text{NO}} = (1 - a) \frac{M_{\text{NO}}}{M_{\text{NO}_2}} \widetilde{\text{NO}}_x$  and  $\widetilde{\text{NO}}_2 = a \widetilde{\text{NO}}_x$ . Thus, we can write

$$\mathbf{c} = \mathbf{f}_s(\widetilde{\text{NO}}, \widetilde{\text{NO}}_2, \widetilde{\text{O}}_3) = \mathbf{g}(\widetilde{\text{NO}}_x), \quad (21)$$

where

where  $\mathbf{g}$  is a function that depends on the  $\widetilde{\text{NO}}_x$  concentration only.

To verify the two-step network model introduced above, we compare it with SIRANE. We note that also the chemical model currently implemented in SIRANE derives from the same assumptions (photostationary equilibrium in the canyon and  $\text{NO}$  and  $\text{O}$  balance). However, differently from SIRANE, we neglect the deposition of chemical species and all the dynamics of dispersion and transformation above roof levels. These assumptions are made to maintain a clear mathematical formulation, in line with the network description. In fact, the fate of the three species is predicted simply by using Eq. (15), i.e. matrix  $A$  from the passive scalar model, and by applying the function  $\mathbf{g}$  for the chemical transformations. To compare the two models, we simulate random emissions of  $\text{NO}_x$  in multiple streets and we compare the resulting concentrations. An emissions ratio  $a = 0.2$  was assigned to the emissions in both models (Carslaw et al., 2016; O'Driscoll et al., 2016; UK National Atmospheric Emission Inventory, 2018). The linear scaling (Eq. (8)) for the wind intensity was used to simulate different speed scenarios starting from a single matrix reconstruction ( $A_0$  for  $U_0 = 5 \text{ m/s}$ ). We find that even in the case of chemical species, the concentrations are predicted with great accuracy for different wind directions and intensities (Figure 7). Although it is not visible from Figure



7.a, the two-step network model gives a slightly higher prediction than SIRANE, about 2% in this data set. These slight deviations are because SIRANE takes into account the deposition of nitrogen oxides while the matrix  $A$  is constructed for a non-depositing passive scalar (see Section 2.2).

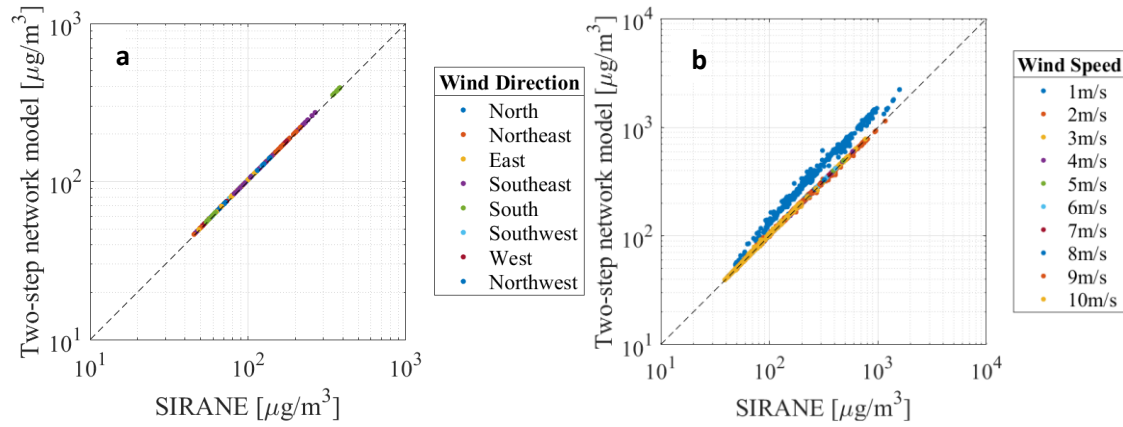


Figure 7: Concentration of  $\text{NO}_2$  in the streets predicted by SIRANE and by the two-step network model introduced in Eqs. (15)–(21). The comparison is made for simulations with different a) wind directions b) and wind speeds.

### 5.1 Calculation of emission sensitivity

The inclusion of chemistry makes the exposure (Section 2.3) a nonlinear function of the emissions  $\mathbf{Q}$ :

$$\mathbf{e} = \mathbf{qp} \circ \mathbf{C} = \mathbf{qp} \circ \mathbf{f}(\tilde{\mathbf{C}}) = \mathbf{qp} \circ \mathbf{f}(B\mathbf{Q}). \quad (22)$$

Exposure variation in the streets due to a change in the pollutant emissions can be expressed as

$$\delta \mathbf{e} = \mathbf{p} \circ \delta \mathbf{C} = \mathbf{p} \circ \delta \mathbf{f}(B\mathbf{Q}), \quad (23)$$

and a Taylor series expansion around the reference emissions  $\mathbf{Q}_0$  results in

$$\delta \mathbf{e} = \mathbf{e} - \mathbf{e}_0 \approx \mathbf{qp} \circ \frac{\partial \mathbf{f}}{\partial \tilde{\mathbf{C}}} B \delta \mathbf{Q}, \quad (24)$$

or simply

$$\delta \mathbf{e} = E \delta \mathbf{Q} \quad \text{where} \quad E = \mathbf{qp} \circ \frac{\partial \mathbf{f}}{\partial \tilde{\mathbf{C}}} B. \quad (25)$$

Recalling that function  $\mathbf{f}$  for a single street is denoted  $\mathbf{f}_s$  for and that it can be simplified to  $\mathbf{g}$  according to Eq. (21), the Jacobian is given by

$$\frac{\partial \mathbf{f}_s}{\partial \tilde{\mathbf{c}}} = \begin{pmatrix} \frac{\partial f_{s,1}}{\partial \tilde{c}_1} & \frac{\partial f_{s,1}}{\partial \tilde{c}_2} & \frac{\partial f_{s,1}}{\partial \tilde{c}_3} \\ \frac{\partial f_{s,2}}{\partial \tilde{c}_1} & \frac{\partial f_{s,2}}{\partial \tilde{c}_2} & \frac{\partial f_{s,2}}{\partial \tilde{c}_3} \\ \frac{\partial f_{s,3}}{\partial \tilde{c}_1} & \frac{\partial f_{s,3}}{\partial \tilde{c}_2} & \frac{\partial f_{s,3}}{\partial \tilde{c}_3} \end{pmatrix} = \frac{d\mathbf{g}}{d\tilde{\text{NO}}_x} \begin{pmatrix} (1-a) \frac{M_{\text{NO}}}{M_{\text{NO}_2}} & a & 0 \end{pmatrix} \quad (26)$$

Figure 8 shows the sensitivity  $d\mathbf{g}/d\tilde{\text{NO}}_x$  for the photochemical equilibrium. Solid lines represent the model feedback when the background concentrations of the case study are considered. Dashed lines refer to the scenario with zero background concentrations. The starting position of the three component curves depends on the background concentration, while the asymptotic value for high  $\tilde{\text{NO}}_x$  concentration depends on the emission ratio  $a$ , i.e. when the emitted and advected nitrogen

oxides ( $\widetilde{NO}_x$ ) are very large, the background concentrations become negligible and the model behaves linearly (constant  $d\mathbf{g}/d\widetilde{NO}_x$ ). We observe that  $d\mathbf{g}/d\widetilde{NO}_x$  for ozone may be negative or positive. The negative(positive)  $d\mathbf{g}/d\widetilde{NO}_x$  occurs when the background concentration of ozone ( $[O_3]_b$ ) is higher(lower) than the ozone concentration at equilibrium ( $[O_3]$ ). In any case, the rate of change of ozone always approaches zero as  $NO_x$  increases. This is due to the consumption of available ozone by nitrogen oxides and can be derived from equations (17)-(18) showing that  $[O_3]$  goes to zero when  $\widetilde{NO}_x$  tends to infinity. Finally, we remark that for the case study considered here, the ozone consumption decreases as the concentration of  $\widetilde{NO}_x$  increases, which raises the risk associated with exposure to ozone (U.S. EPA, 2020).

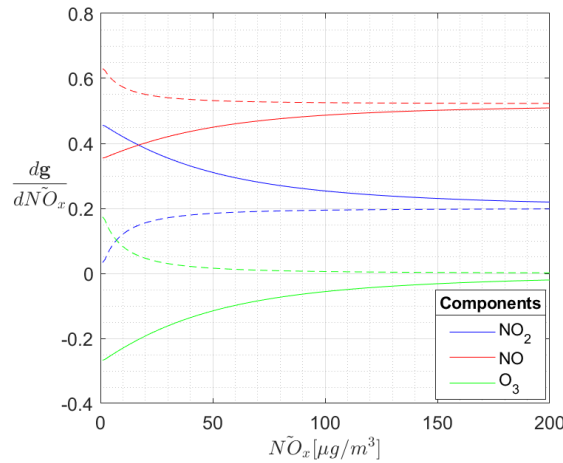
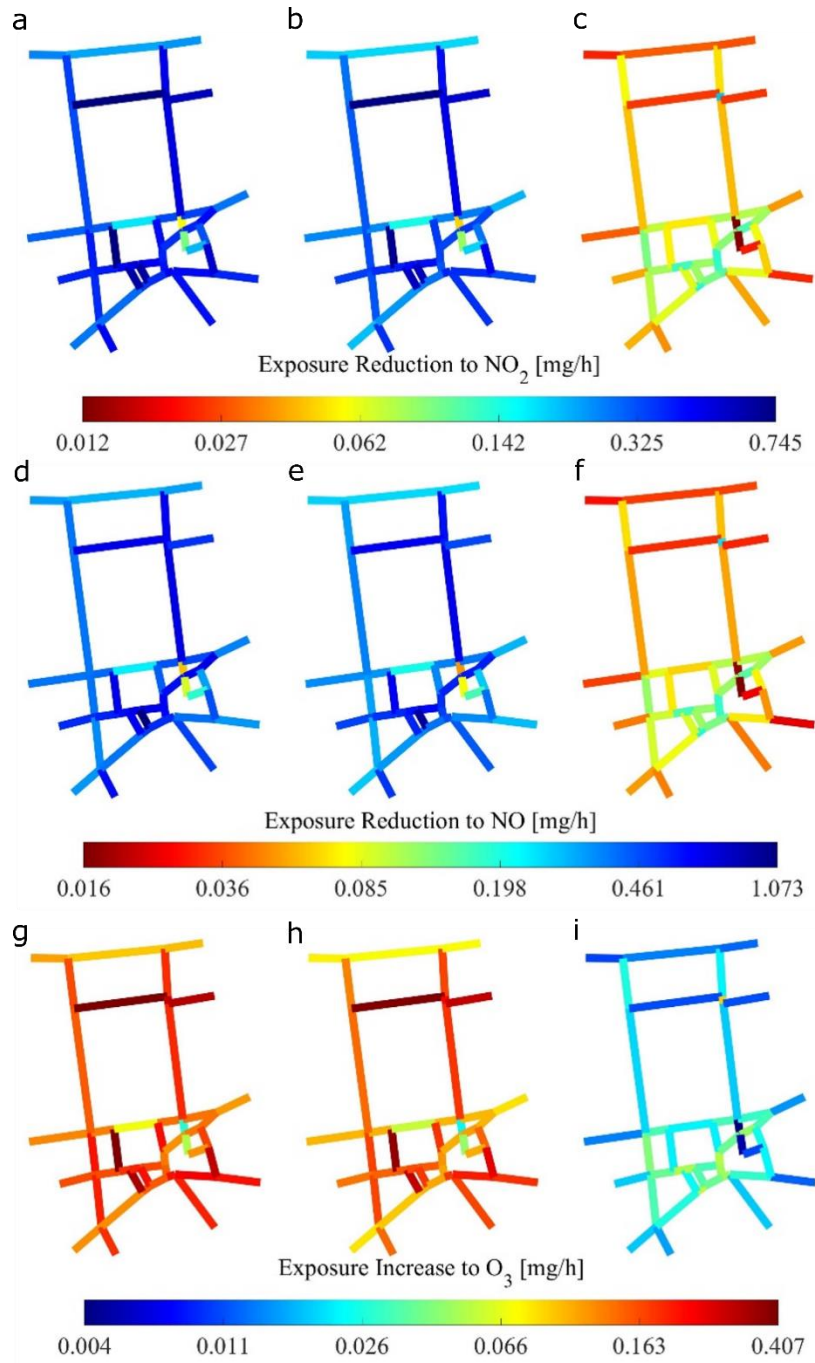


Figure 8 : Sensitivity of  $NO_2$ ,  $NO$  and  $O_3$  concentration to the increase in the  $\widetilde{NO}_x$  concentration according to Eq. (21). Zero background concentrations (dashed lines) and background concentrations of the case study ( $NO_2 = 34.26 \mu g/m^3$ ,  $NO = 17.09 \mu g/m^3$ ,  $O_3 = 27.31 \mu g/m^3$ , solid lines).

## 5.2 Where to reduce emissions?

By substituting the emission sensitivity (26) into Eq. (25), it is straightforward to construct the emission matrix  $E$  for the scenario with photochemical smog and therefore the exposure reduction  $R$  by means of Eq. (12). Below,  $R$  is used to identify the best places to reduce emissions in the urban network. As in section 4.4, an emissions variation  $\delta Q = 0.10 \bar{Q}$  is considered for both  $NO$  and  $NO_2$  emissions (as the emissions ratio  $\alpha$  is constant).

426  
427



428  
429  
430  
431  
432

Figure 9: Exposure reduction achieved by decreasing the emission in the street by a constant quantity  $\delta Q$  for  $\text{NO}_2$  (a-c) and  $\text{NO}$  (d-f). For  $\text{O}_3$  the increase in exposure is shown in (g-i). (a,d,g) and (b,e,h) show the maximum and average values for the different wind directions. (c,f,i) show the average computed by neglecting self-interactions. Note the colorbar employs a logarithmic scaling.

433

434  
435  
436

Figure 9 shows the exposure reduction or increase for  $\text{NO}_2$ ,  $\text{NO}$ , and  $\text{O}_3$ , in the South Kensington case study. As expected, a reduction  $\delta Q$  in  $\text{NO}_x$  emissions leads to an exposure reduction to nitrogen oxides (Panels a-f). The results are very similar to the passive scalar case (Figure 5), and can nearly be

reproduced using a single scaling factor per species. This is due to two reasons: (i) the relation between  $\text{NO}_2$  and  $\widetilde{\text{NO}}_2$  in the photostationary model is almost linear, especially for large  $\widetilde{\text{NO}}_2$  concentration (see Figure 8); and (ii) the background concentration and the ratio  $\alpha$  are kept constant for all the streets. Consequently  $d\mathbf{g}/d\widetilde{\text{NO}}_x$  has almost constant entries and the matrix  $E$  in Eq. (25) is simply rescaled with respect to the case of the passive scalar.

On the other hand, panels g-i in Figure 9 evidence an exposure increase to ozone. This is in line with Figure 8 which shows a negative  $d\mathbf{g}/d\widetilde{\text{NO}}_x$  for ozone in the case study (solid lines). As explained above, this negative rate depends on the relation between the background and equilibrium ozone concentration. This result highlights that a side effect of the reduction of vehicular traffic may be an increase in ozone concentrations, depending on the background concentrations present in the area.

Finally, we remark that the sensitivity analysis presented in this section is dependent on the case study not only due to the dependence of  $d\mathbf{g}/d\widetilde{\text{NO}}_x$  on the background concentration but also for its dependence on the initial emissions in the streets which provide  $\widetilde{\text{NO}}_x$  concentration (see Eqs. (14)-(15)).

## Conclusions

In this work a complex network approach was used to address what is the optimal place to reduce emissions in an urban neighbourhood. Rather than developing a new air quality model, we introduced a mathematical formalism inspired by the theory of complex networks and based on the analysis of physical mechanisms, capable of extending the potential of existing operational tools. In fact, thanks to our approach, it is ultimately possible to reconstruct a large multiplicity of scenarios starting from a single dispersion simulation of a passive scalar.

The network was defined by modelling the correlation between emissions and concentrations in streets as weighted links connecting the streets, i.e. the nodes of the network. In this way, the entire process of pollutant dispersion was enclosed in the weight matrix  $A$  of the network. By means of this formulation the hypothesis of linearity between emissions and concentrations in the case of non-reactive pollutants was first tested. Then, considering the physics underlying the process, we proposed a linear scaling of matrix  $A$  with the intensity of the external wind. In this way, scenarios with different emissions in the streets and different intensity of the external wind could be reproduced using a single weight matrix  $A_0$  constructed from a single dispersion simulation. The network model highlighted the diagonal-dominancy of the problem and suggested a criterion to significantly reduce the computational complexity of the solution, eliminating the less significant network connections.

The network description facilitated straightforward translation from polluting concentrations to citizen exposure: a new weight matrix, the exposure matrix, was derived starting from  $A$  which took into account the number of people exposed in each street. The outdegree of this new matrix provided a direct metric for exposure reduction in terms of which streets bring the greatest benefits in terms of health impact at the neighbourhood scale.

Finally, the model was extended to the analysis of photochemical smog. We used a two-step algorithm to reconstruct the concentrations of reactive pollutants in the streets by applying matrix  $A$  and a non-linear function for chemical transformations in the streets. Through a linearization of the exposure model, we obtained an expression of the exposure reduction metric for reacting chemical species and we showed that it can be approximated with a rescaling of the metric for the passive case.

The exposure model used in combination with the diagonal dominance of  $A$  gave clear indication of what generally the most effective strategy is in terms of health: to reduce emissions in domestic

streets with the high aspect ratio  $H/W$ , e.g. by making the street one-way. Indeed, the exposure estimate in Eq. (13) is an accurate measure that can be used to estimate total exposure in a street in an operational sense without even the need for a network model.

The work presented in this manuscript is straightforward to extend to much larger urban areas, and it is recommended study more realistic emission reduction scenarios, e.g. considering emissions reductions in multiple streets rather than a single street. Further research in the application of metrics and techniques from the theory of complex networks can bring new insights into the analysis of the results and guide administrations in traffic and emission management.

## Acknowledgements

The authors would like to thank Prof. Lionel Soulhac for providing a custom version of SIRANE suitable for source apportionment and for insightful conversations about data assimilation.

## Bibliography

- Anenberg, S. C., Moheggh, A., Goldberg, D. L., Kerr, G. H., Brauer, M., Burkart, K., Hystad, P., Larkin, A., Wozniak, S., & Lamsal, L. (2022). Long-term trends in urban NO<sub>2</sub> concentrations and associated paediatric asthma incidence: estimates from global datasets. *The Lancet Planetary Health*, 6(1), e49–e58. [https://doi.org/10.1016/S2542-5196\(21\)00255-2](https://doi.org/10.1016/S2542-5196(21)00255-2)
- Baker, J., Walker, H. L., & Cai, X. (2004). A study of the dispersion and transport of reactive pollutants in and above street canyons—a large eddy simulation. *Atmospheric Environment*, 38(39), 6883–6892.
- Barthelemy, M. (2016). *The structure and dynamics of cities*. Cambridge University Press.
- Batty, M. (2013). *The new science of cities*. MIT press.
- Berkowicz, R. (2000). OSPM-A parameterised street pollution model. *Environmental Monitoring and Assessment*, 65(1–2), 323–331.
- Bloomberg, L., & Dale, J. (2000). Comparison of VISSIM and CORSIM Traffic Simulation Models on a Congested Network. *Transportation Research Record: Journal of the Transportation Research Board*, 1727(1), 52–60. <https://doi.org/10.3141/1727-07>
- Boccaletti, S., Latora, V., Moreno, Y., Chavez, M., & Hwang, D.-U. (2006). Complex networks: Structure and dynamics. *Physics Reports*, 424(4–5), 175–308.
- Bright, V. B., Bloss, W. J., & Cai, X. (2013). Urban street canyons: Coupling dynamics, chemistry and within-canyon chemical processing of emissions. *Atmospheric Environment*, 68, 127–142.
- Carpentieri, M., Salizzoni, P., Robins, A., & Soulhac, L. (2012). Evaluation of a neighbourhood scale, street network dispersion model through comparison with wind tunnel data. *Environmental Modelling and Software*, 37, 110–124. <https://doi.org/10.1016/j.envsoft.2012.03.009>
- Clappier, A., Belis, C. A., Pernigotti, D., & Thunis, P. (2017). Source apportionment and sensitivity analysis: two methodologies with two different purposes. *Geoscientific Model Development*, 10(11), 4245–4256. <https://doi.org/10.5194/gmd-10-4245-2017>

Derwent, R. G., & Middleton, D. R. (1996). An empirical function for the ratio NO<sub>2</sub>: NO<sub>x</sub>.  
*Clean Air*, 26(3), 57–60.

EEA. (2022). *Managing air quality in Europe*.

Epa, U., & Factors Program, E. (2011). *Exposure Factors Handbook: 2011 Edition*. www.epa.gov

Fellini, S., Salizzoni, P., & Ridolfi, L. (2020). Centrality metric for the vulnerability of urban networks to toxic releases. *Physical Review E*, 101(3), 32312.

Fellini, S., Salizzoni, P., & Ridolfi, L. (2021). Vulnerability of cities to toxic airborne releases is written in their topology. *Scientific Reports*, 11(1). <https://doi.org/10.1038/s41598-021-02403-y>

Fellini, S., Salizzoni, P., Soulhac, L., & Ridolfi, L. (2019). Propagation of toxic substances in the urban atmosphere: A complex network perspective. *Atmospheric Environment*, 198, 291–301.

Greater London Authority. (n.d.). *London Average Air Quality Levels - London Datastore*. Retrieved April 1, 2022, from <https://data.london.gov.uk/dataset/london-average-air-quality-levels>

Grewe, V., Tsati, E., & Hoor, P. (2010). On the attribution of contributions of atmospheric trace gases to emissions in atmospheric model applications. *Geoscientific Model Development*, 3(2), 487–499. <https://doi.org/10.5194/gmd-3-487-2010>

Grylls, T., le Cornec, C. M. A., Salizzoni, P., Soulhac, L., Stettler, M. E. J., & van Reeuwijk, M. (2019). Evaluation of an operational air quality model using large-eddy simulation. *Atmospheric Environment: X*, 3, 100041. <https://doi.org/10.1016/J.AEAOA.2019.100041>

Iacobello, G., Marro, M., Ridolfi, L., Salizzoni, P., & Scarsoglio, S. (2019). Experimental investigation of vertical turbulent transport of a passive scalar in a boundary layer: Statistics and visibility graph analysis. *Physical Review Fluids*, 4(10), 104501.

Int Panis, L., Broekx, S., & Liu, R. (2006). Modelling instantaneous traffic emission and the influence of traffic speed limits. *Science of The Total Environment*, 371(1–3), 270–285. <https://doi.org/10.1016/j.scitotenv.2006.08.017>

Kakosimos, K. E., Hertel, O., Ketzel, M., & Berkowicz, R. (2010). Operational Street Pollution Model (OSPM) - a review of performed application and validation studies, and future prospects. *Environmental Chemistry*, 7(6), 485. <https://doi.org/10.1071/EN10070>

Khreis, H., Kelly, C., Tate, J., Parslow, R., Lucas, K., & Nieuwenhuijsen, M. (2017). Exposure to traffic-related air pollution and risk of development of childhood asthma: A systematic review and meta-analysis. In *Environment International* (Vol. 100, pp. 1–31). Elsevier Ltd. <https://doi.org/10.1016/j.envint.2016.11.012>

Kim, Y., Wu, Y., Seigneur, C., & Roustan, Y. (2018). Multi-scale modeling of urban air pollution: development and application of a Street-in-Grid model (v1. 0) by coupling MUNICH (v1. 0) and Polair3D (v1. 8.1). *Geoscientific Model Development*, 11(2), 611–629.

Koo, B., Wilson, G. M., Morris, R. E., Dunker, A. M., & Yarwood, G. (2009). Comparison of Source Apportionment and Sensitivity Analysis in a Particulate Matter Air Quality Model. *Environmental Science & Technology*, 43(17), 6669–6675. <https://doi.org/10.1021/es9008129>

Lu, J., Li, B., Li, H., & Al-Barakani, A. (2021). Expansion of city scale, traffic modes, traffic congestion, and air pollution. *Cities*, 108, 102974. <https://doi.org/10.1016/j.cities.2020.102974>



557 McHugh, C. A., Carruthers, D. J., & Edmunds, H. A. (1997). ADMS-Urban: an air quality management  
558 system for traffic, domestic and industrial pollution. In *Int. J. Environment and Pollution* (Vol. 8).

559 McHugh, C. A., Carruthers, D. J., & Edmunds, H. A. (1997). ADMS-Urban: an air quality management  
560 system for traffic, domestic and industrial pollution. *International Journal of Environment and*  
561 *Pollution*, 8(3–6), 666–674.

562 Newman, M. (2010). *Networks*. Oxford University Press.  
563 <https://doi.org/10.1093/acprof:oso/9780199206650.001.0001>

564 Oke, T. R., Mills, G., Christen, A., & Voogt, J. A. (2017). *Urban Climates*. Cambridge University Press.  
565 <https://doi.org/10.1017/9781139016476>

566 Park, N. (2020). Population-estimates-for-the-UK-England-and-Wales-Scotland-and-Northern-  
567 Ireland-provisional-mid-2019. *Hampshire: Office for National Statistics*.

568 Salizzoni, P., Soulhac, L., & Mejean, P. (2009). Street canyon ventilation and atmospheric turbulence.  
569 *Atmospheric Environment*, 43(32), 5056–5067.  
570 <https://doi.org/10.1016/j.atmosenv.2009.06.045>

571 Ser-Giacomi, E., Baudena, A., Rossi, V., Vasile, R., Lopez, C., & Hernández-Garca, E. (2019). From  
572 network theory to dynamical systems and back: Lagrangian Betweenness reveals bottlenecks in  
573 geophysical flows. *ArXiv Preprint ArXiv:1910.04722*.

574 Soulhac, L., Nguyen, C. v., Volta, P., & Salizzoni, P. (2017). The model SIRANE for atmospheric urban  
575 pollutant dispersion. PART III: Validation against NO<sub>2</sub> yearly concentration measurements in a  
576 large urban agglomeration. *Atmospheric Environment*, 167, 377–388.  
577 <https://doi.org/10.1016/j.atmosenv.2017.08.034>

578 Soulhac, L., Puel, C., Duclaux, O., & Perkins, R. J. (2003). Simulations of atmospheric pollution in  
579 Greater Lyon an example of the use of nested models. *Atmospheric Environment*, 37(37), 5147–  
580 5156. <https://doi.org/10.1016/j.atmosenv.2003.03.002>

581 Soulhac, L., & Salizzoni, P. (2010). Dispersion in a street canyon for a wind direction parallel to the  
582 street axis. *Journal of Wind Engineering and Industrial Aerodynamics*, 98(12), 903–910.  
583 <https://doi.org/10.1016/j.jweia.2010.09.004>

584 Soulhac, L., Salizzoni, P., Cierco, F. X., & Perkins, R. (2011a). The model SIRANE for atmospheric urban  
585 pollutant dispersion; part I, presentation of the model. *Atmospheric Environment*, 45(39),  
586 7379–7395.

587 Soulhac, L., Salizzoni, P., Cierco, F. X., & Perkins, R. (2011b). The model SIRANE for atmospheric  
588 urban pollutant dispersion; part I, presentation of the model. *Atmospheric Environment*,  
589 45(39), 7379–7395. <https://doi.org/10.1016/j.atmosenv.2011.07.008>

590 Soulhac, L., Salizzoni, P., Cierco, F.-X., & Perkins, R. (2011c). The model SIRANE for atmospheric  
591 urban pollutant dispersion; part I, presentation of the model. *Atmospheric Environment*,  
592 45(39), 7379–7395.

593 Soulhac, L., Salizzoni, P., Mejean, P., Didier, D., & Rios, I. (2012). The model SIRANE for atmospheric  
594 urban pollutant dispersion; PART II, validation of the model on a real case study. *Atmospheric*  
595 *Environment*, 49, 320–337. <https://doi.org/10.1016/j.atmosenv.2011.11.031>

596 UK Ambient Air Quality Interactive Map. (n.d.). Retrieved April 1, 2022, from [https://uk-](https://uk-air.defra.gov.uk/data/gis-mapping/)  
597 [air.defra.gov.uk/data/gis-mapping/](https://uk-air.defra.gov.uk/data/gis-mapping/)

598 U.S. EPA. (2020). *Integrated Science Assessment (ISA) for Ozone and Related Photochemical Oxidants*  
599 *(Final Report, Apr 2020)*.

600 Wagstrom, K. M., Pandis, S. N., Yarwood, G., Wilson, G. M., & Morris, R. E. (2008). Development and  
601 application of a computationally efficient particulate matter apportionment algorithm in a  
602 three-dimensional chemical transport model. *Atmospheric Environment*, 42(22), 5650–5659.  
603 <https://doi.org/10.1016/J.ATMOENV.2008.03.012>

604 Wang, Z. S., Chien, C.-J., & Tonnesen, G. S. (2009). Development of a tagged species source  
605 apportionment algorithm to characterize three-dimensional transport and transformation of  
606 precursors and secondary pollutants. *Journal of Geophysical Research*, 114(D21).  
607 <https://doi.org/10.1029/2008jd010846>

608 WHO. (2021). *WHO global air quality guidelines: particulate matter (PM2.5 and PM10), ozone,*  
609 *nitrogen dioxide, sulfur dioxide and carbon monoxide*.

610 Wu, Y., Zhang, S., Hao, J., Liu, H., Wu, X., Hu, J., Walsh, M. P., Wallington, T. J., Zhang, K. M., &  
611 Stevanovic, S. (2017). On-road vehicle emissions and their control in China: A review and  
612 outlook. *Science of The Total Environment*, 574, 332–349.  
613 <https://doi.org/10.1016/J.SCITOTENV.2016.09.040>

614 Zhang, K., Chen, G., Zhang, Y., Liu, S., Wang, X., Wang, B., & Hang, J. (2020). Integrated impacts of  
615 turbulent mixing and NO<sub>x</sub>-O<sub>3</sub> photochemistry on reactive pollutant dispersion and intake  
616 fraction in shallow and deep street canyons. *Science of the Total Environment*, 712, 135553.

617